THE JOURNAL OF PHYSICAL CHEMISTRY C

Article

Cite This: J. Phys. Chem. C 2019, 123, 17624−17631

pubs.acs.org/JPCC

Tunable Sorting of Mesoscopic Chiral Structures by External Noise in Achiral Periodic Potentials

Jie Su, Hui-Jun Jiang,* and Zhong-Huai Hou*

Department of Chemical Physics & Hefei National Laboratory for Physical Sciences at the Microscale, University of Science and Technology of China, Hefei 230026, China

Supporting Information

ABSTRACT: Efficient chirality sorting is now highly in demand to separate assembled mesoscopic chiral structures which are of very special physical properties rather than their achiral counterparts or those at the single-particle level. However, the efficiency of conventional methods usually suffers from the thermal or external noise. Here, we propose a mechanism utilizing external noise to attain a tunable sorting of mesoscopic chiral particles in an achiral periodic potential. The complete chirality separation stems from the path selection by a noise-induced biased flux in a nonequilibrium landscape. Such a mechanism provides a practical way to control the motion of chiral particles by simply adjusting the noise intensity, which is demonstrated by simultaneous separation of several kinds of enantiomorphs with different degrees of chirality. The robustness and generalizability of noise-tuned chirality sorting is further verified in systems with other types of periodic potentials or spatially/temporally correlated noise.

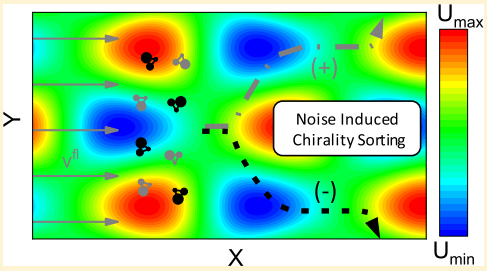

INTRODUCTION

Chirality is a property of mirror asymmetry essential in several branches of science.[1−3] Very recently, explosive attention has been paid to mesoscopic chiral structures assembled from micro- or mesoblocks.[4−10] Such assembled chiral structures are shown to be of very special optical, electric, or magnetic properties rather than their achiral counterparts or those at the single-particle level.[4−8] Because the assembled products are usually mixtures of enantiomorphs,[4,8] methods to efficiently sort such chiral structures then receive great research interest.

So far, several types of chirality-sorting methods have been proposed. Usually, a system with intrinsic chirality along the separation direction, for instance, asymmetric shear flow,[11−16] helical flow field,[17−19] and some materials such as chirality-separation sieves,[20−22] can be utilized to sort chiral objects. Interestingly, periodic potentials without intrinsic chirality can also be used to separate enantiomorphs, thus providing a more convenient way for chirality sorting. In the pioneer work done by de Gennes,[23] a macroscopic chiral crystal was found to glide in a direction differing slightly from the axis of maximum slope when it was slipping over an inclined solid support. For separation of smaller chiral objects such as macromolecules or assembled mesoscopic structures where thermal fluctuation is non-negligible, it was argued that the fluctuation would destroy this effect.[23] In terms of this, many efforts have been paid to search for efficient chirality sorting methods against thermal noise.[24−26] Speer et al. demonstrated that the two chiral counterparts can even move into opposite directions with remarkable persistence against thermal noise with the help of periodic potentials.[24] Similarly, particles that only differ by their chirality were also found to migrate along different directions when driven by a steady fluid flow through a square lattice of cylindrical posts when thermal noise presents.[25] Furthermore, it has also been reported that periodic potentials can display not only chirality separation but also the ability to steer particles to arbitrary locations.[26] One should note that, for a real system, thermal fluctuations are inevitable, which are related to the dissipation process such as friction via a fluctuation−dissipation theorem. Such thermal fluctuations may be regarded as "internal" to the system dynamics. In addition, the system's dynamics may also be influenced by noises from the environment or external fields. However, many studies have shown that external noise can play constructive roles in nonlinear dynamic systems and lead to counterintuitive phenomena, such as stochastic resonance.[27−31] Therefore, it is very interesting to ask whether external noise can also be favorable for chirality sorting rather than destroying it. Because external noise is unavoidable in real systems and may be tuned systematically, the answer to this question may provide new methods to achieve tunable chirality sorting.

Here, we establish a two-dimensional noise-tuned system consisting of assembled chiral particles driven by flowing fluid in an achiral periodic potential. As a result, an optimal chirality sorting with complete chirality-separation and an interesting rollover phenomenon are observed by solely adjusting the noise intensity. Analysis based on nonequilibrium landscape and flux theory reveals that, within the nonequilibrium landscape, a noise-induced biased flux would guide particles

Received: May 23, 2019
Revised: June 21, 2019
Published: June 24, 2019

DOI: 10.1021/acs.jpcc.9b04882
J. Phys. Chem. C 2019, 123, 17624−17631

of a given chirality to move along a selected direction, leading to the optimal chirality separation with 100% selectivity as well as the interesting rollover of chirality sorting. Detailed analysis on dynamical trajectories finds that the biased flux is generated by a noise-induced path transition, which may be further associated with the intrinsic dynamical asymmetry of enantiomorphs. More interestingly, the selected direction shows a quantitative dependence on the noise intensity, revealing a tunable motion of chiral particles by external noise. Based on the mechanism, simultaneous separation of several kinds of enantiomorphs with different degrees of chirality is successfully realized. The robustness and generalizability of noise-tuned chirality sorting in systems with other types of periodic potentials or spatially/temporally correlated noise are further verified. Thus, our method provides a conceptually new and practicable way for tunable chirality sorting in real systems.

MODEL AND METHODS

We consider a mesoscopic two-dimensional chiral structure as an equilateral trilateral particle with side length l_0 assembled by three rigidly coupled nanoparticles located at $\mathbf{r}_i$, i = 1, 2, 3 (Figure 1). The chirality of the particle is realized by setting

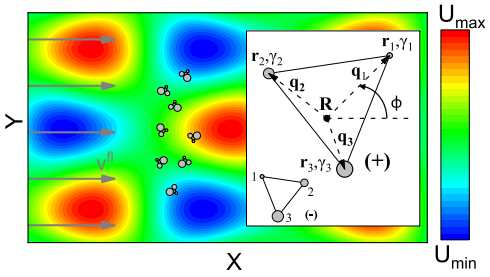

Figure 1. Schematic of the chiral particles driven by a fluid field v^{fl} (gray arrows) through an achiral periodic potential $U(r)$ (colored background). The inset is the zoom-in of a pair of chiral particles. The (+) particle consists of three nanoparticles arranged counterclockwise with $\gamma_1 < \gamma_2 < \gamma_3$ on an equilateral triangle's vertexes $\mathbf{r}_i$. $\mathbf{R}$ is the center of friction and ϕ is the angle between the vector $\mathbf{r}_1 - \mathbf{R}$ and the X axis. The (−) particle differs only in that the sequence of γ_is is clockwise.

the three nanoparticles to be of different sizes, which consequently results in different friction coefficients γ_i.[12,17] Taking $\gamma_1 < \gamma_2 < \gamma_3$, we consider a particle is of (+) chirality if the first, second, and third nanoparticles (nodes) are arranged counterclockwise and is of (−) chirality for clockwise arrangement (the inset in Figure 1). The state of such a rigid particle can then be described by the position of its friction center $\mathbf{R} = \sum_{i=1}^{3}\gamma_i\mathbf{r}_i/\sum_{i=1}^{3}\gamma_i$ and by the orientation angle ϕ between the vector $\mathbf{r}_1 - \mathbf{R}$ and the X axis. The position of each nanoparticle can be determined by $\mathbf{r}_i = \mathbf{R} + \mathbf{q}_i(\phi) = \mathbf{R} + \mathbf{O}(\phi)\mathbf{q}_i^{(0)}$, where $\mathbf{q}_i$ is the vector pointing from $\mathbf{R}$ to node-i, $\mathbf{q}_i^{(0)}$ denotes its value in a reference configuration with $\phi = 0$, and $\mathbf{O}(\phi)$ is a rotation matrix whose elements are $O_{11} = O_{22} = \cos(\phi)$ and $O_{21} = -O_{12} = \sin(\phi)$. Then, the friction center evolution can be calculated by the motions of the three nanoparticles,[17,24] that is, the particle obeys the coupled Langevin equations as follows

$$\frac{d\mathbf{R}(t)}{dt} = \frac{\sum_{i=1}^{3}\mathbf{F}(\mathbf{r}_i) + \sum_{i=1}^{3}\gamma_i\mathbf{v}^{fl}(\mathbf{r}_i)}{\sum_{i=1}^{3}\gamma_i} + \boldsymbol{\xi}(t) + \boldsymbol{\zeta}(t) \quad (1)$$

$$\frac{d\phi(t)}{dt} = \frac{\mathbf{e}_z\cdot\sum_{i=1}^{3}\mathbf{q}_i(\phi)\times[\mathbf{F}(\mathbf{r}_i) + \gamma_i v^{fl}(\mathbf{r}_i)]}{\sum_{i=1}^{3}\gamma_i|\mathbf{q}_i|^2} + \xi_\phi(t) + \zeta_\phi(t) \quad (2)$$

Herein, $\mathbf{F}(\mathbf{r}_i) = -\nabla U(\mathbf{r}_i)$ denotes the force exerted to node-i, where

$$U(\mathbf{r}) = C\gamma\sum_{j=1}^{3} c_j\cos(K\hat{k}_j\cdot r + \delta_j) \quad (3)$$

is the periodic potential taken as a superposition of three standing waves,[26] with C the potential strength, K the inverse spatial scale, and $\hat{k}_j$, c_j, δ_j, respectively, the unit vector, ratio, and phase offset associated with the j-th standing wave ($\sum_{j=1}^{3}c_j^2 = 1$). Such a potential may be realized by an external electric or optical field.[26,32] We fix $c_1 = 0.256$, $c_2 = c_3 = 0.683$, $\hat{k}_1 = (1, 0)$, $\hat{k}_2 = (-0.5, 3/2)$, $\hat{k}_3 = (0.5, 3/2)$, $\delta_1 = 0$, $\delta_2 = 2.49$, and $\delta_3 = 3.79$, such that the maxima and minima of the potential lie on interpenetrating triangular lattices (Figure 1). The potential has mirror symmetry parallel to the X axis, but none parallel to the Y axis.

In eq 1, $\mathbf{v}^{fl}(\mathbf{r}_i) = v_0\mathbf{e}_x$ denotes a velocity field of a fluid with constant speed v_0, which provides driven force for particle movement along the X axis. $\boldsymbol{\xi}(t)$ is thermal noise which can be expressed as an independent Gaussian white noise satisfying the fluctuation−dissipation relation $\langle\boldsymbol{\xi}_\mu(t)\boldsymbol{\xi}_\nu(t')\rangle = 2\gamma_c^{-1}k_BT\delta(t - t')\delta_{\mu\nu}$, where the subscript $\mu(\nu)$ denotes the component along the $X(Y)$ axis, k_B is the Boltzmann constant, T denotes the temperature, and $\gamma_c = \sum_{i=1}^{3}\gamma_i$ represents the total friction coefficient. $\boldsymbol{\zeta}(t)$ is an external noise with $\langle\boldsymbol{\zeta}_\mu(t)\boldsymbol{\zeta}_\nu(t')\rangle = 2D_e\delta(t - t')\delta_{\mu\nu}$, where the intensity D_e can be tuned, externally. Equation 2 represents the rotation of the chiral particle, where torques are exerted by $\mathbf{F}$ and $\gamma_i\mathbf{v}^{fl}$. The scalar $|\mathbf{q}_i|$ is the norm of $\mathbf{q}_i$, as well as $\xi_\phi(t)$ and $\zeta_\phi(t)$ are the internal and external rotational fluctuation, respectively, satisfying $\langle\xi_\phi(t)\xi_\phi(t')\rangle = 2k_BTr_\gamma^{-2}\delta(t - t')$, $\langle\zeta_\phi(t)\zeta_\phi(t')\rangle = 2D_e\gamma_c r_\gamma^{-2}\delta(t - t')$, where $r_\gamma = (\sum_{i=1}^{3}\gamma_i|\mathbf{q}_i|^2)^{1/2}$ is independent of ϕ and represents an invariant property of the molecule.[17]

In simulations, parameters are made dimensionless by using l_0, γ_1, and v_0 as the basic units. Accordingly, the basic unit for time is l_0/v_0 that for energy is $l_0v_0\gamma_1$. We fix $K = 0.3$, $C = 6.67$, and $k_BT = 10^{-5}$ all through the present work. For consistency, all of the following results are obtained from particles running for a long time $t = 10^6$ with 2×10^4 randomly chosen initial states with different orientations near the origin. In the following, we mainly focus on the dynamics of (+) particles, because the behaviors of (−) particles are the same except that their motions are symmetric to those of (+) ones with respect to the X-axis.

RESULTS AND DISCUSSION

We now investigate how the external noise influences chirality sorting of particles with $\gamma_1 = 1.0$, $\gamma_2 = 1.5$ and $\gamma_3 = 2.0$. Typical trajectories for $D_e = 0$, 10^{-4}, and 0.1 are shown in the insets of Figure 2, respectively. Without noise ($D_e = 0$, the top-left inset in Figure 2), both enantiomorphs can move along two different paths, one of which along the positive Y-direction (named as the positive path, Movie S1) and the other with a negative one (the negative path, Movie S2). Nevertheless, trajectories for (+) and (−) particles are mixed with each other, so that the two enantiomorphs cannot be separated. Quite interestingly, for a moderate noise intensity $D_e = 10^{-4}$(the bottom inset in

DOI: 10.1021/acs.jpcc.9b04882
J. Phys. Chem. C 2019, 123, 17624−17631

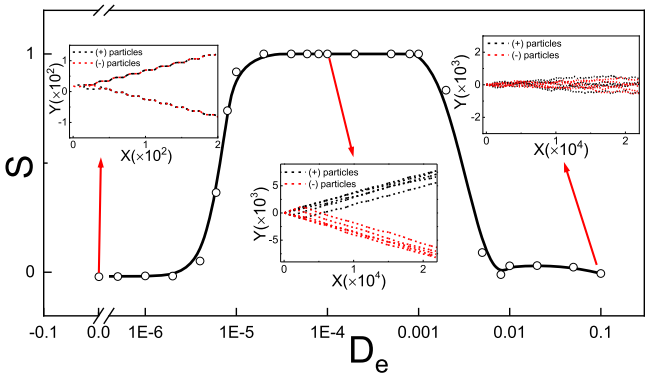

Figure 2. Optimal chirality sorting induced by the external noise. Chirality selectivity S as a function of the external noise intensity D_e for $\gamma_1 = 1.0$, $\gamma_2 = 1.5$, and $\gamma_3 = 2.0$. The top-left, bottom, and top-right insets are typical trajectories of the $(\pm)$ particles for $D_e = 0$, 10^{-4}, and 0.1, respectively.

Figure 2), all of the (+) particles move along the positive path while all (−) particles along the negative one, resulting in two well-separated clusters of particles, wherein the two enantiomorphs are nearly 100% sorted. If the noise intensity becomes large enough, for instance $D_e = 0.1$ (the top-right inset in Figure 2), (+) and (−) particles are mixed again.

The above observation clearly indicates that external noise can induce chirality sorting, and there exists an optimal level of noise intensity that may most favorably enhance the sorting selectivity. In order to quantitatively characterize such an effect, we may introduce an order parameter S to measure the chirality selectivity as

$$S = \int_0^\infty P_{(+)}(Y)\mathrm{d}Y - \int_0^\infty P_{(-)}(Y)\mathrm{d}Y \tag{4}$$

where $P_{(\pm)}(Y)$ denotes the probability distribution of the final Y-position for the $(\pm)$ particles. For $S > 0$ ($S < 0$), (+) particles distribute more(less) above the X axis than (−) particles. $S = 0$ means that no chirality sorting can be observed, while for $S = \pm 1$ the two enantiomorphs can be separated completely. The obtained S as a function of D_e is presented in Figure 2. It is observed that chirality selectivity depends non-monotonically on the intensity of the external noise, and at an optimal noise intensity, a complete sorting with 100% chirality selectivity can be realized.

In order to understand the underlying mechanism of the interesting observations aforementioned, we now try to figure out the nonequilibrium potential landscape and flux for the

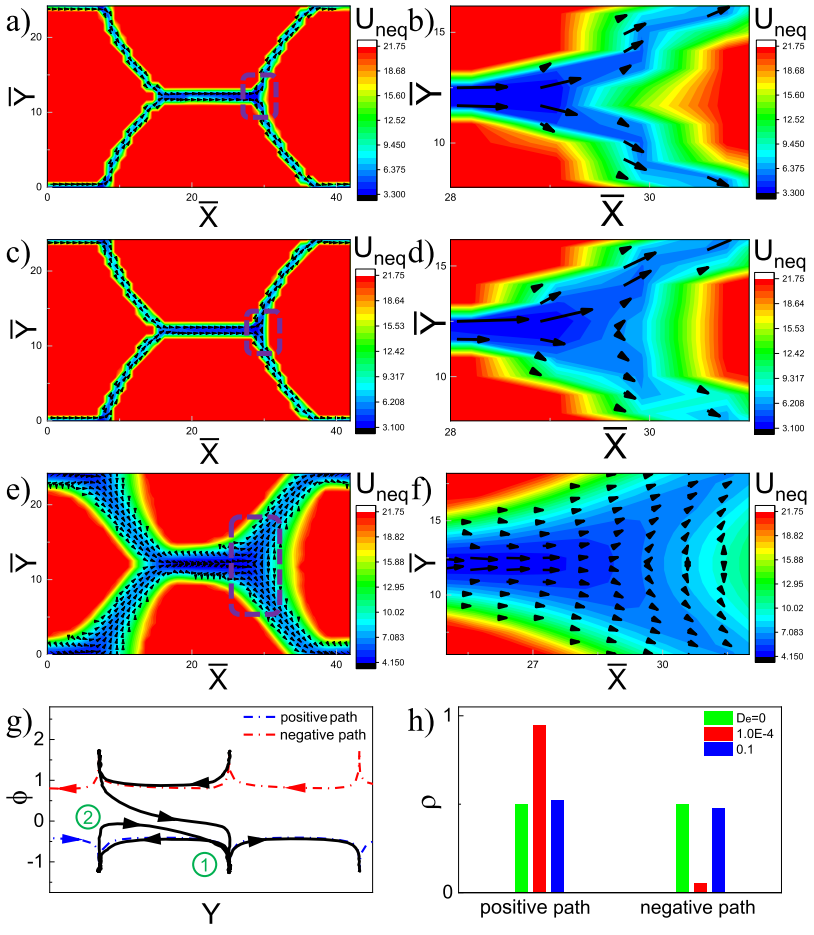

Figure 3. Underlying mechanism for the noise-induced chirality sorting. (a,c,e) Nonequilibrium landscape (colored background) and flux vectors (arrows representing the directions of flux) of the (+) particle for external noise intensity $D_e = 0$, 10^{-4}, and 0.1. (b,d,f) Zoom-in of the purple boxes in (a,c,e), respectively (the length of arrows representing the strength of flux). (g) Dominant transition (the multistep transition) of (+) particles from the negative to the positive path. The blue and red lines show the positive and the negative path, respectively. Arrows are the moving direction of particles. (h) Probabilities ρ of how long the (+) particles stay in the positive and negative paths.

DOI: 10.1021/acs.jpcc.9b04882
J. Phys. Chem. C 2019, 123, 17624−17631

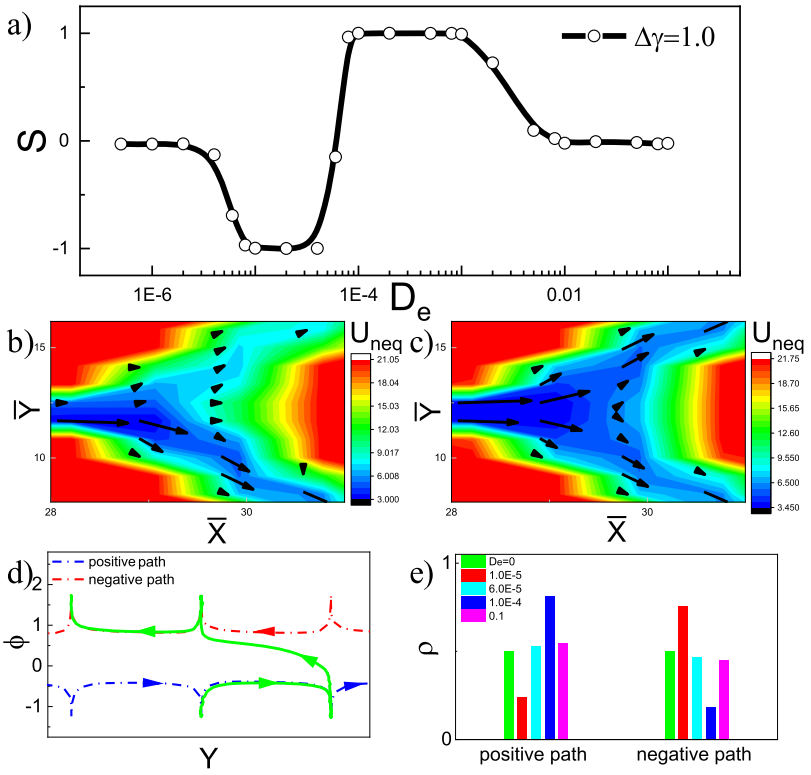

Figure 4. Chirality sorting and underlying mechanism for chirality sorting with $\Delta\gamma = 1.0$. (a) Chirality selectivity S as a function of the external noise intensity D_e. (b,c) Nonequilibrium landscape (colored background) and flux vectors (arrows and its length representing the directions and strength of flux) of the (+) particle with $\Delta\gamma = 1.0$ for external noise intensity $D_e = 10^{-5}$ and 10^{-4}. (d) Dominant transition (the direct transition) of (+) particles from the negative to the positive path for $S = -1$. The blue and red lines show the positive and the negative path, respectively. Arrows are the moving direction of particles. (e) Probabilities ρ of how long the (+) particles stay in the positive and negative paths for $\Delta\gamma = 1.0$.

periodic positions of chiral particles in a lattice of the potential at different noise intensities. Generally, the evolution equation of the friction center can be written as $d\bar{\mathbf{R}}/dt = f(\bar{\mathbf{R}}) + \xi_{\bar{\mathbf{R}}}(t)$, where $\bar{\mathbf{R}} = (\bar{X}, \bar{Y})$ is the periodic position of the friction center in a lattice of the potential, that is, $\bar{X}(t) = \mathrm{mod}(X(t),L_X)$, $\bar{Y}(t) = \mathrm{mod}(Y(t),L_Y)$ with L_X and L_Y the periodic length of the given potential. $f(\bar{\mathbf{R}})$ is a deterministic force and $\xi_{\bar{\mathbf{R}}}(t)$ is a random force satisfying $\langle \xi_{\bar{\mathbf{R}}}(t)\xi_{\bar{\mathbf{R}}}(t')\rangle = 2D\delta(t - t')$ with D the corresponding diffusion coefficient. Via the Fokker−Plank equation for the probability distribution $P(\bar{X},\bar{Y})$, the nonequilibrium potential landscape and flux can then be well defined as $U_{\mathrm{neq}}(\bar{X},\bar{Y}) = -\ln P_{\mathrm{SS}}$, $J_{\mathrm{SS},\bar{X}}(\bar{X},\bar{Y}) = f(\bar{X},\bar{Y})P_{\mathrm{SS}} - D\partial P_{\mathrm{SS}}/\partial\bar{X}$, and $J_{\mathrm{SS},\bar{Y}}(\bar{X},\bar{Y}) = f(\bar{X},\bar{Y})P_{\mathrm{SS}} - D\partial P_{\mathrm{SS}}/\partial\bar{Y}$,[33] where the subscript SS represents the steady state (see details in the Supporting Information).

By applying the above analysis on the (+) particle, the nonequilibrium landscape (colored background) and flux vectors (arrows) for typical external noise intensity D_e are depicted in Figure 3a−f. For $D_e = 0$ (Figure 3a,b), two paths lying in the valleys of the nonequilibrium landscape with fluxes symmetric with respect to the X axis can be observed, corresponding to the two moving paths observed in the inset of Figure 2. However, with the increasing noise intensity, the flux becomes no more symmetric (e.g., for $D_e = 10^{-4}$ shown in Figure 3c,d). It is obvious that the flux vectors pointing to the positive direction are much larger than those pointing to the negative one. Consequently, the biased flux will drive (+) particles moving along the positive path, rather than the negative one, leading to complete chirality sorting ($S = 1$). As the noise intensity further increases to be large enough (such as $D_e = 0.1$ in Figure 3e,f), the landscape becomes much more flat and the flux recovers to be symmetric again, implying a mixed state ($S = 0$) dominated by the noise. In short, for an appropriate intensity of the external noise, the biased-flux-induced moving direction selection of the chiral particles leads to the observed optimal chirality sorting with 100% chirality selectivity.

Herein, the origin of the biased flux occurring in the achiral potential turns into an interesting question. We find that a pair of particle with same chirality cannot move symmetrically with respect to the X axis because their bead positions, centers of friction, and orientation angles are impossible to maintain symmetric simultaneously, which leads to different forces or torques exerting on the particles and eventually breaks the symmetric motion at the particle level (see details in Supporting Information). Besides, it is observed that the (+) particle always oscillates its ϕ below 0 periodically along the positive path (the blue line in Figure 3g) and above 0 along the negative one (the red line in Figure 3g). The ranges of oscillation along these two paths are asymmetric with respect to $\phi = 0$, indicating an intrinsic dynamical asymmetry at the trajectory level. More interestingly, a noise-induced reversible transition between the positive and negative paths can be observed for $D_e > 5.0 \times 10^{-6}$ (the black line in Figure 3g), along which the (+) particle on the negative(positive) path first jumps to a state with opposite sign of ϕ while still keeping the negative(positive) moving direction (Step ① 1 in Figure 3g), then changes its moving direction oppositely and along the positive (negative) one (Step ② 2 in Figure 3g, Movies S3 and S4). Thus, such a transition can be named as the multistep

DOI: 10.1021/acs.jpcc.9b04882
J. Phys. Chem. C 2019, 123, 17624−17631

transition. To present how the multistep transition affects the particle distribution along the positive and negative paths, the probability ρ of how long the (+) particle stays along the two paths is plotted in Figure 3h. When noise is absent or too large, the (+) particle moves along both of the paths with equal probabilities (green and blue bars in Figure 3h). For moderate noise intensity (such as $D_e = 10^{-4}$), the (+) particle prefers to stay much longer along the positive path than the negative one (red bars in Figure 3h), indicating a biased flux driving (+) particle moving from the negative path to the positive one at the path-transition level. Therefore, we argue that the asymmetrical flux is generated by a noise-induced path transition, which may be further associated with the intrinsic dynamical asymmetry of enantiomorphs.

We investigate whether the chirality sorting of enantiomorphs can be tuned by D_e for other arrangement of values for γ_is. Then, we use the parameter $\Delta\gamma \equiv \gamma_3 - \gamma_2 = \gamma_2 - \gamma_1$ to characterize the degree of chirality for chiral particles by setting the difference between two consequent γ_is to be the same. For $\Delta\gamma = 1.0$, that is, $\gamma_1 = 1.0$, $\gamma_2 = 2.0$, and $\gamma_3 = 3.0$, dependence of S on D_e is plotted in Figure 4a. Similar to the one for $\Delta\gamma = 0.5$, S is nearly 0 for $D_e < 5.0 \times 10^{-6}$. In contrast to the situation for $\Delta\gamma = 0.5$, S decreases quickly to $S = -1$ as D_e increases to be slightly larger than 5.0×10^{-6}, indicating a chirality sorting with all of the (+) particles only distributed below the X axis. Remarkably, by further increasing D_e ($>6.0 \times 10^{-5}$), a rollover of chirality sorting is observed, that is, S increases rapidly from -1 to 1. In both of the parameter regions where $|S| = 1$, chiral particles are separated completely while moving path of the (+) particles is the negative one for $S = -1$ and the positive one for $S = 1$. As D_e increases to be large enough, S drops back to 0 again. In short, for $\Delta\gamma = 1.0$, similar noise-induced optimal chirality sorting with 100% selectivity can also be achieved, along with a new noise-induced rollover of chirality sorting.

The interesting observation can be understood based on the nonequilibrium potential landscape and flux analysis, too (Figures 4b,c and S2). Similar to $\Delta\gamma = 0.5$, the flux symmetric with respect to the X axis can be observed at small or large noise intensity. For noise intensity in between, it is a little complicated. As D_e increases to be slightly larger than 5.0×10^{-6} (such as $D_e = 10^{-5}$, Figure 4b), the flux to the negative direction is much larger than that to the positive one, so that the biased flux would drive (+) particles moving along the negative path, in contrast to the situation for $\Delta\gamma = 0.5$. By further increasing D_e to be, such as, $D_e = 10^{-4}$ (Figure 4c), the flux to the positive direction becomes larger in comparison with that to the negative direction, in accordance with the rollover from $S = -1$ to $S = 1$ aforementioned. In other words, noise can further induce a change of the "flux direction" for $\Delta\gamma = 1.0$, leading to the observation of noise-induced rollover of optimal chirality sorting.

We are now interested in why the flux direction can be changed. As discussed in the chirality sorting for $\Delta\gamma = 0.5$, the biased flux originates from the intrinsic dynamical asymmetry of the chiral particles and the noise-induced transition between the moving paths. Notice that the intrinsic dynamical asymmetry still holds for $\Delta\gamma = 1.0$; thus, the transition between the moving paths is focused in following analysis. For small noise intensity (such as $D_e = 10^{-5}$), a new type of dominant reversible transition is observed. As indicated by the green line in Figure 4d, the (+) particle jumps from the positive path to the negative one directly (named as the direct transition, Movies S5 and S6). It is found that, via the direct transition, the (+) particle prefers to distribute along the negative path (red bars in Figure 4e), and thus, the direct transition would result in a biased flux mainly pointing to the negative direction. For large D_e, it is observed that a multistep transition similar to the one for $\Delta\gamma = 0.5$ emerges and dominates the path transition process, which forces the (+) particle to distribute mainly along the positive path (blue bars in Figure 4e), leading to another type of biased flux preferring to pointing to the positive direction. In between, there is a mixed state for $D_e = 6.0 \times 10^{-5}$ as depicted by the nearly equal-height cyan bars in Figure 4e, where chiral particles cannot be separated. In short, noise-shifted dominant transition between particle-moving paths is the very reason for the changing of the flux direction for $\Delta\gamma = 1.0$.

Based on the revealed physics, we expect to explore the possibility for noise-controlled moving directions of chiral particles. The most probable moving directions of (+) particles $\theta_m = \langle \lim_{t\to\infty} \mathrm{atan}(Y(t)/X(t)) \rangle$ as functions of the external noise intensity D_e with $\Delta\gamma = 0.5$ and 1.0 are presented in Figure 5a. It is observed that θ_m can be tuned quantitatively from 0.42 to 0 for $\Delta\gamma = 0.5$ by increasing D_e (the black line in

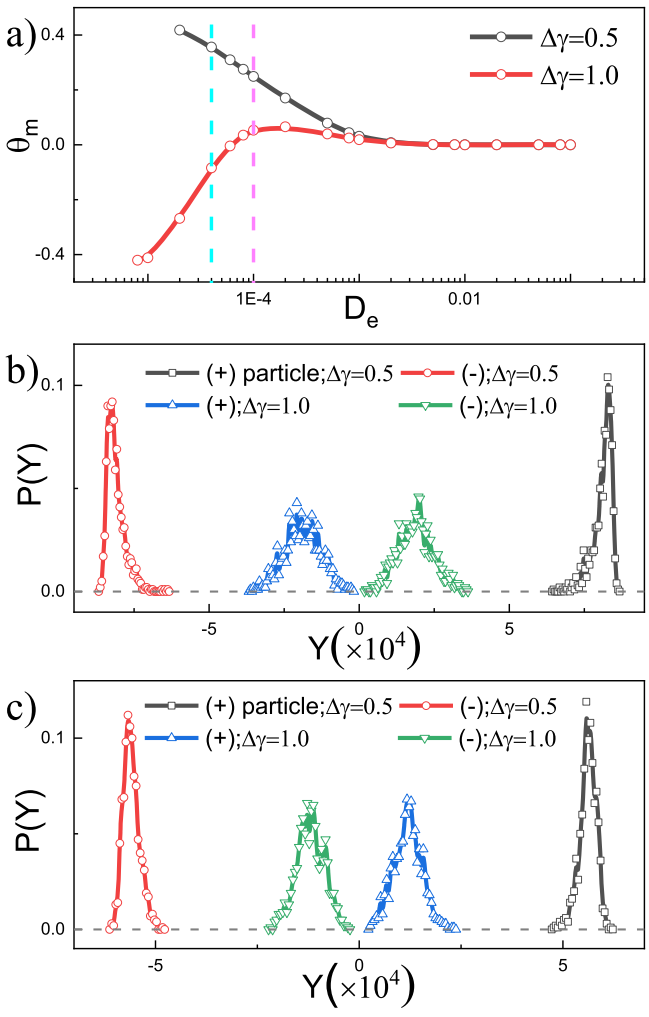

Figure 5. Noise-induced tunable chirality sorting. (a) Most probable moving direction θ_m of the (+) particle for $\Delta\gamma = 0.5$ and 1.0. (b,c) Simultaneous chirality sorting for different kinds of enantiomorphs. Distributions on the Y-position for four different chiral particles with $\Delta\gamma = 0.5$ and 1.0 for external noise intensity $D_e = 4.0 \times 10^{-5}$ and 1.0×10^{-4} (cyan and magenta dashed lines in (a)).

DOI: 10.1021/acs.jpcc.9b04882
J. Phys. Chem. C 2019, 123, 17624−17631

Figure 5a). Similarly, θ_m for $\Delta\gamma = 1.0$ can also be tuned from −0.42 to 0.07 then back to 0 with increasing D_e (the red line in Figure 5a). In comparison with that for $\Delta\gamma = 0.5$, not only the value of θ_m, but also the sign can be tuned by solely changing D_e. Thus, it is possible for us to guide chiral particles to some given positions by solely tuning the intensity of external noise, which provides a more powerful tool for applications in real systems beyond the noise-induced chirality sorting.

More interestingly, one should note that different values of $|\theta_m|$ mean different final positional distributions of chiral particles, so it is possible for us to provide a potential routine to separate not only a pair of enantiomorphs with the same degree of chirality but also many kinds of enantiomorphs with different $\Delta\gamma$, simultaneously. To validate this idea, the distribution $P(Y)$ of four different chiral particles (two kinds of enantiomorphs with $\Delta\gamma = 0.5$ and 1.0) is shown in Figure 5b,c for $D_e = 4.0 \times 10^{-5}$ and 10^{-4}, corresponding to the cyan and magenta dashed lines in Figure 5a, respectively. Clearly, for both D_e, all of these four kinds of particles fall in different areas on the Y axis without any overlap, indicating that all these four kinds of particles can be separated perfectly at the same time.

To fully explore how parameters affect the chirality sorting, the phase diagram in the $D_e-\Delta\gamma$ plane is obtained (Figure 6).

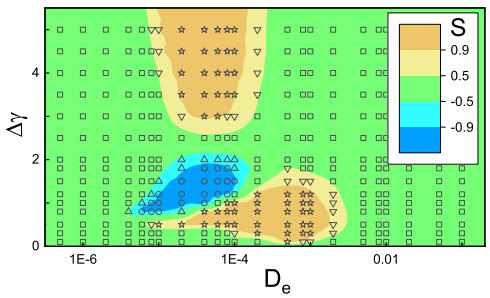

Figure 6. Phase diagram for chirality sorting in the $D_e-\Delta\gamma$ plane. Circles and stars: complete separation state. Triangles: partial separation state. Squares: mixed state. The (+) particles prefer to move along the positive direction in yellow domains, while they tend to move along the negative one in blue domains.

There are several states which can be observed in the phase diagram. In the complete separation state (both of the dark blue and dark yellow domains), chiral particles can be completely separated as $|S| \approx 1$, while (+) particles move along the positive direction in the dark yellow domain and along the negative direction in the dark blue one. Chiral particles can only be partially separated in the partial separation state (the light blue and light yellow domains) and cannot be separated at all in the mixed state (the light green domain). For both $\Delta\gamma$ less than 0.8 and $\Delta\gamma$ larger than 2.5, chirality selectivity depends non-monotonically on the intensity of the external noise. Such optimal chirality sorting behavior can be observed for very large $\Delta\gamma$ (even for $\Delta\gamma >$ 100). For $\Delta\gamma$ in between, noise-induced rollover of chirality selectivity occurs. This complete phase diagram consisting of various states enables feasibilities for many new chirality sorting routines in practice.

To explore the generalizability of the noise-tuned chirality sorting, chirality sorting in different types of periodic potentials and with different types of noises is also investigated by intensive simulations. Figure 7a,b shows the chirality selectivity S as functions of noise intensity D_e in two periodic potentials of other shapes (see details in Supporting Information). Obviously, an optimal chirality sorting with 100% selectivity can also be induced by the external noise in these potentials. We have also observed that chirality sorting would not happen when the potential is uniform along the direction parallel or vertical to the flowing fluid. Combined with the potential lying on interpenetrating triangular lattices aforementioned, we argue that chirality sorting could still be observed if the potential is periodic both along the X axis (the flowing direction) and the Y axis (vertical to the flowing direction), while other details of the potential such as the shape seems to be irrelevant.

To further validate the concept of noise-tuned chirality sorting in systems of correlated noise (experimentally controlled noise is usually correlated), similar simulations are performed by replacing the external white noise by time-correlated or space-correlated noise (see Supporting Information for details). The external time-correlated noise $\mathbf{g}(t)$ is

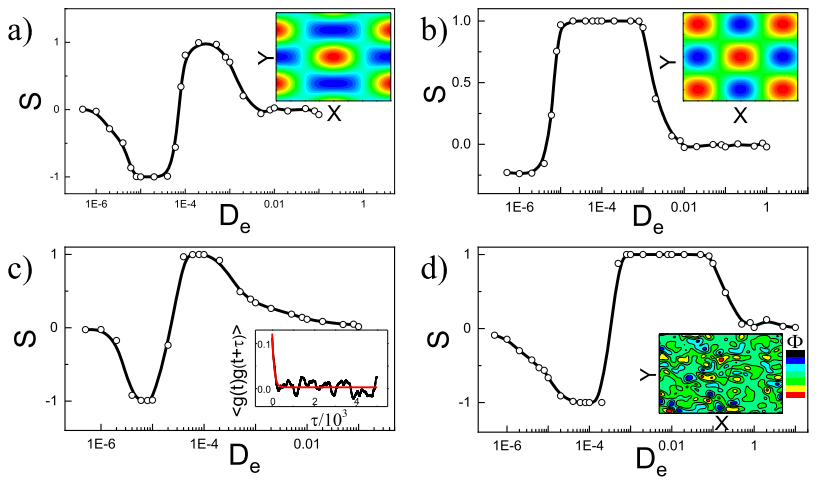

Figure 7. Generalizability of noise-tuned chirality sorting. Chirality selectivity S as functions of D_e with $\Delta\gamma = 1.0$ for (a,b) periodic potentials with different shapes, and (c) time- or (d) space-correlated noises. Insets in (a,b): periodic potentials of different shapes. Inset in (c): correlation function of the time-correlated noise (the black line) and its exponential fit (the red line). Inset in (d): a typical snapshot of two-dimensional random space-correlated noise field. Corresponding values of the fields in the insets of (a,b,d) increase as the color changes from blue to red.

DOI: 10.1021/acs.jpcc.9b04882
J. Phys. Chem. C 2019, 123, 17624−17631

chosen as Ornstein−Uhlenbeck noise, whose correlation function $\langle \mathbf{g}(t)\mathbf{g}(t + \Delta t)\rangle = D_e\, e^{-\Delta t/\tau_p}$ (inset of Figure 7c), where τ_p is the characteristic time scale of the correlation. The space-correlated noise requires the construction of a random noise field $\Phi(\mathbf{x},t)$ (inset of Figure 7d).[34] As expected, chirality sorting and its rollover can be observed with these kinds of noises, too (Figure 7c,d). Besides, the finite correlation time(scale) of such correlated noise further offers a rich parameter space for tunable chirality sorting, which may be systematically investigated in future works.

CONCLUSIONS

In summary, we found an optimal sorting of mesoscopic chiral particles occurring with the help of external noise in an achiral periodic potential. The moving direction of chiral particles can be well controlled by the intensity of external noise, leading to a conceptually new noise-tuned chirality-sorting method. Such an interesting effect originates from a biased flux driving particles to move along a selected direction, which is generated by the noise-induced path transition. The robustness and generalizability of noise-tuned chirality sorting were further demonstrated in systems with other types of potentials or spatially/temporally correlated noise. Compared with conventional separation methods, the noise-tuned sorting of mesoscopic chiral structures, on the one hand, broadens our ability of chirality sorting for practical purposes where other methods may fail and, on the other hand, provides a new basic concept for tunable chirality sorting by utilizing the constructive role of external noise. For instance, we demonstrated that, based on the noise-tuned moving directions of chiral particles, it is possible to simultaneously separate several types of enantiomorphs just by adapting the intensity of external noise solely. Because external noise is independent of the internal properties of the systems and can be conveniently controlled than internal noise, our method may open a brand-new perspective on both theoretical and experimental investigations of tunable sorting of chiral structures assembled from micro- or mesoblocks in the future.

ASSOCIATED CONTENT

Supporting Information

The Supporting Information is available free of charge on the ACS Publications website at DOI: 10.1021/acs.jpcc.9b04882.

Intrinsic dynamical asymmetry of enantiomorphs; non-equilibrium landscape and flux vectors of the (+) particle; correlated external noise-induced chirality sorting for particles with different chirality degrees; and typical snapshot of the two-dimensional space-correlated noise field for chiral particles (PDF)

Positive path for the (+) particle (AVI)

Negative path for the (+) particle (AVI)

First type of the multistep transition for the (+) particle (AVI)

Second type of the multistep transition for the (+) particle (AVI)

First type of the direct transition for the (+) particle (AVI)

Second type of the direct transition for the (+) particle (AVI)

AUTHOR INFORMATION

Corresponding Authors

*E-mail: hjjiang3@ustc.edu.cn (H.-J.J.).
*E-mail: hzhlj@ustc.edu.cn (Z.-Z.H.).

ORCID

Zhong-Huai Hou: 0000-0003-1241-7041

Author Contributions

H.-J.J. and Z.-H.H. conceived the idea and supervised the research. J.S. performed the simulations and data analysis. All authors discussed the results and the underlying mechanism and co-wrote the manuscript.

Notes

The authors declare no competing financial interest.

ACKNOWLEDGMENTS

We acknowledge valuable discussions with Prof. Jin Wang. This work is supported by MOST (2016YFA0400904, 2018YFA0208702), NSFC (21833007, 21790350, 21673212, 21521001, 21473165), the Fundamental Research Funds for the Central Universities (2340000074), and Anhui Initiative in Quantum Information Technologies (AHY090200).

REFERENCES

(1) Gal, J. Molecular Chirality in Chemistry and Biology: Historical Milestones. *Helv. Chim. Acta* **2013**, *96*, 1617.

(2) Ariëns, E. J. Stereochemistry, a Basis for Sophisticated Nonsense in Pharmacokinetics and Clinical Pharmacology. *Eur. J. Clin. Pharmacol.* **1984**, *26*, 663.

(3) Eichelbaum, M.; Gross, A. S. *Stereochemical Aspects of Drug Action and Disposition*; Advances in Drug Research; Academic Press, 1996; Vol. *28*, pp 1−64.

(4) Ma, F.; Wang, S.; Wu, D. T.; Wu, N. Electric-Field-Induced Assembly and Propulsion of Chiral Colloidal Clusters. *Proc. Natl. Acad. Sci. U.S.A.* **2015**, *112*, 6307.

(5) Zhang, H.; Xin, X.; Sun, J.; Zhao, L.; Shen, J.; Song, Z.; Yuan, S. Self-assembled chiral helical nanofibers by amphiphilic dipeptide derived from d - or l -threonine and application as a template for the synthesis of Au and Ag nanoparticles. *J. Colloid Interface Sci.* **2016**, *484*, 97.

(6) Mark, A. G.; Gibbs, J. G.; Lee, T.-C.; Fischer, P. Hybrid Nanocolloids with Programmed Three-Dimensional Shape and Material Composition. *Nat. Mater.* **2013**, *12*, 802.

(7) McPeak, K. M.; van Engers, C. D.; Blome, M.; Park, J. H.; Burger, S.; Gosálvez, M. A.; Faridi, A.; Ries, Y. R.; Sahu, A.; Norris, D. J. Complex Chiral Colloids and Surfaces via High-Index Off-Cut Silicon. *Nano Lett.* **2014**, *14*, 2934.

(8) Shen, X.; Zhan, P.; Kuzyk, A.; Liu, Q.; Asenjo-Garcia, A.; Zhang, H.; García de Abajo, F. J.; Govorov, A.; Liu, N.; Liu, N. 3D Plasmonic Chiral Colloids. *Nanoscale* **2014**, *6*, 2077.

(9) Zhang, J.; Granick, S. Natural Selection in the Colloid World: Active Chiral Spirals. *Faraday Discuss.* **2016**, *191*, 35.

(10) Schamel, D.; Pfeifer, M.; Gibbs, J. G.; Miksch, B.; Mark, A. G.; Fischer, P. Chiral Colloidal Molecules and Observation of the Propeller Effect. *J. Am. Chem. Soc.* **2013**, *135*, 12353.

(11) Eichhorn, R. Microfluidic Sorting of Stereoisomers. *Phys. Rev. Lett.* **2010**, *105*, 034502.

(12) Eichhorn, R. Enantioseparation in Microfluidic Channels. *Chem. Phys.* **2010**, *375*, 568.

(13) Marcos; Fu, H. C.; Powers, T. R.; Stocker, R. Separation of Microscale Chiral Objects by Shear Flow. *Phys. Rev. Lett.* **2009**, *102*, 158103.

(14) Talkner, P.; Ingold, G.-L.; Hänggi, P. Transport of Flexible Chiral Objects in a Uniform Shear Flow. *New J. Phys.* **2012**, *14*, 073006.

DOI: 10.1021/acs.jpcc.9b04882
J. Phys. Chem. C 2019, 123, 17624−17631

(15) Makino, M.; Doi, M. Migration of Twisted Ribbon-Like Particles in Simple Shear Flow. *Phys. Fluids* **2005**, *17*, 103605.
(16) Meinhardt, S.; Smiatek, J.; Eichhorn, R.; Schmid, F. Separation of Chiral Particles in Micro- or Nanofluidic Channels. *Phys. Rev. Lett.* **2012**, *108*, 214504.
(17) Kostur, M.; Schindler, M.; Talkner, P.; Hänggi, P. Chiral Separation in Microflows. *Phys. Rev. Lett.* **2006**, *96*, 014502.
(18) Aristov, M.; Eichhorn, R.; Bechinger, C. Separation of Chiral Colloidal Particles in a Helical Flow Field. *Soft Matter* **2013**, *9*, 2525.
(19) Beleke-Maxwell, K.; Franke, T.; Hoppe, R. H. W.; Linsenmann, C. Numerical Simulation of Surface Acoustic Wave Actuated Enantiomer Separation by the Finite Element Immersed Boundary Method. *Comput. Fluids* **2015**, *112*, 50.
(20) Gabashvili, A.; Medina, D. D.; Gedanken, A.; Mastai, Y. Templating Mesoporous Silica with Chiral Block Copolymers and Its Application for Enantioselective Separation. *J. Phys. Chem. B* **2007**, *111*, 11105.
(21) Wang, P.-X.; Hamad, W. Y.; MacLachlan, M. J. Polymer and Mesoporous Silica Microspheres with Chiral Nematic Order from Cellulose Nanocrystals. *Angew. Chem., Int. Ed.* **2016**, *55*, 12460.
(22) Bueno-Perez, R.; Balestra, S. R. G.; Camblor, M. A.; Min, J. G.; Hong, S. B.; Merkling, P. J.; Calero, S. Influence of Flexibility on the Separation of Chiral Isomers in STW-Type Zeolite. *Chem.—Eur. J.* **2018**, *24*, 4121.
(23) de Gennes, P. G. Mechanical Selection of Chiral Crystals. *Europhys. Lett.* **1999**, *46*, 827.
(24) Speer, D.; Eichhorn, R.; Reimann, P. Exploiting Lattice Potentials for Sorting Chiral Particles. *Phys. Rev. Lett.* **2010**, *105*, 090602.
(25) Bogunovic, L.; Fliedner, M.; Eichhorn, R.; Wegener, S.; Regtmeier, J.; Anselmetti, D.; Reimann, P. Chiral Particle Separation by a Nonchiral Microlattice. *Phys. Rev. Lett.* **2012**, *109*, 100603.
(26) Nourhani, A.; Crespi, V. H.; Lammert, P. E. Guiding Chiral Self-Propellers in a Periodic Potential. *Phys. Rev. Lett.* **2015**, *115*, 118101.
(27) Wiesenfeld, K.; Moss, F. Stochastic Resonance and the Benefits of Noise: from Ice Ages to Crayfish and SQUIDs. *Nature* **1995**, *373*, 33.
(28) Faisal, A. A.; Selen, L. P. J.; Wolpert, D. M. Noise in the Nervous System. *Nat. Rev. Neurosci.* **2008**, *9*, 292 , and references therein .
(29) Hänggi, P. Stochastic Resonance in Biology How Noise Can Enhance Detection of Weak Signals and Help Improve Biological Information Processing. *ChemPhysChem* **2002**, *3*, 285 , and references therein .
(30) Xin, H. Theoretical Study on Stochastic Resonance in Chemical Systems. *Chin. J. Chem. Phys.* **2000**, *13*, 388.
(31) Hänggi, P.; Marchesoni, F. Artificial Brownian Motors: Controlling Transport on the Nanoscale. *Rev. Mod. Phys.* **2009**, *81*, 387.
(32) Khan, S. A.; Shi, Y.; Chang, C.-M.; Jan, C.; Fan, S.; Ellerbee, A. K.; Solgaard, O. Optical Separation of Heterogeneous Size Distributions of Microparticles on Silicon Nitride Strip Waveguides. *Opt. Express* **2015**, *23*, 8855.
(33) Wang, J.; Xu, L.; Wang, E. Potential Landscape and Flux Framework of Nonequilibrium Networks: Robustness, Dissipation, and Coherence of Biochemical Oscillations. *Proc. Natl. Acad. Sci. U.S.A.* **2008**, *105*, 12271.
(34) Milotti, E. Trajectories of Brownian Particles with Space-Correlated Noise. *J. Chem. Sci.* **2017**, *129*, 983.

DOI: 10.1021/acs.jpcc.9b04882
J. Phys. Chem. C 2019, 123, 17624−17631